Ab initio theoretical study of the structure and electronic spectra of Co^{2+} in $KZnF_3$

José Luis Pascual
Departamento de Química Física Aplicada, C-14 Universidad Autónoma de Madrid, 28049 Madrid, Spain
(Received 29 October 2002; published 19 March 2003)

In this paper we present the results of *ab initio* model potential embedded cluster calculations on $(CoF_6)^{4-}$ in the lattice of $KZnF_3$ to model theoretically the different electronic spectra (absorption, emission and excited state absorption spectroscopies) of Co^{2+}-doped $KZnF_3$, a transition-metal ion laser system. By the use of the *ab initio* model potential method, the main nonrelativistic effects (correlation, embedding effects) as well as scalar and spin-orbit relativistic effects are included in the calculations, providing a reliable description of the different spectra. As a first step toward the determination of the spectra, geometries around the impurity as well as vibrational frequencies are determined for the ground state and a number of electronic excited states. The spectra themselves present an excellent overall agreement with the experimental findings both for absorption and emission spectroscopies. Based on this good agreement, we are able to make a revision of the excited state absorption experiments, concluding that Jahn-Teller effects are important in the interpretation of the spectrum, and suggesting an assignment for the lower-energy band of this spectrum. The implications of these facts in the laser capacity of the material are also discussed.

DOI: 10.1103/PhysRevB.67.115112 PACS number(s): 71.55.−i, 31.15.−p, 78.55.Hx

I. INTRODUCTION

Transition-metal ions doped into ionic lattices are materials of technological interest due to their luminiscent properties, especially as solid-state lasers.[1,2] A great variety of dopant ions and host lattices have been explored as candidates, and numerous examples of actual working lasers have been found. Among them, lasers formed when ions with a d^3 or d^7 electronic structure are doped into ionic lattices are interesting for their tunability and their possibilities for high-temperature performance.[3–6] Co^{2+} as a dopant in $KZnF_3$ belongs to this group and has been demonstrated to lase efficiently,[7,8] in a range of energies (between 1.70 and 2.10 μm) of practical interest.

A good knowledge of the general spectral properties of the materials is necessary for a detailed understanding of the laser properties and an accurate prediction of potential systems. To this end, experimental studies have been conducted in the past to analyze absorption and emission[7,9,10] as well as excited-state absorption (ESA) (Ref. 9) of Co^{2+}:$KZnF_3$. In particular, the ESA spectrum is a very interesting task, since a competition between the ESA and emission can exist in these materials, and has been proved to be very detrimental to the laser performance in related systems.[11] The experimental results have been analyzed using approximate treatments, such as the single-configuration coordinate (SCC).[12] The success of this type of study, very useful for studies of temperature-dependent decays, relies on the existence of a large amount of very precise experimental information, from which the key parameters (vibrational mode energies, Huang-Rhys parameters, etc.) can be obtained free of uncertainties. This fact is more important in the case of excited-state studies.[13]

In this context, theoretical studies acquire a special importance. By using high level techniques that include all the relevant interactions, information complementary to the experimental information can be obtained, so that the analysis of the spectral information can be better performed and experimental uncertainties could be solved reliably. Examples of this kind of theoretical calculation applied to the systems formed by V^{2+} and Cr^{3+} in fluoroperovskites can be found in Refs. 14–17, where assignments of spectral features were made and schemes proposed to ease the understanding of some controversial points. These studies and some other related demonstrated the ability of the so-called *ab initio* model potential (AIMP) method to provide valuable information on these materials.[18]

Following this line, in this paper we present an AIMP embedded cluster study of the spectral properties of the laser material Co^{2+}:$KZnF_3$. We find some problems in the interpretation of the experimental spectra (absorption, emission, ESA) performed previously, and propose assignments coherent with the experimental information available that should have some influence on the lasing activity of the material. To sum up, very different values are reported for the parameters relevant to the interpretation of the spectrum [vibrational energies, Huang-Rhys factors (S)] depending on the different experiments.[7,9] Using them, SCC diagrams are constructed and used to interpret the electronic spectra. From this analysis, the bands in the ESA spectrum are assigned, and their width is explained by strong spin-orbit mixings that we do not find consistent with our calculations. The SCC diagrams themselves display some features not consistent with ligand-field theory intuition. We give reliable values for the different spectral parameters, and propose an interpretation of the ESA spectrum, based on the possibility of different Jahn-Teller effects for the different excited states and on the existence of multiple-state absorptions in the spectrum.

$KZnF_3$ is a crystal of the fluoroperovskite family. In it, the Zn^{2+} ion is surrounded by six F^- anions that form a perfect octahedron around it. When doped with divalent cations, the dopant ion (Co^{2+} in this case), substitutes for the Zn^{2+} ion, in an octahedral environment. The Co^{2+} dopant ion has a d^7 electronic structure and, in a fluoride lattice like $KZnF_3$, the weak-field $t_{2g}^5 e_g^2$ configuration is the most stable one, giving a $^4T_{1g}$ ground state. The transitions from this ground state to

the first excited states (those lying up to 30 000 cm^{-1} from the ground state) constitute the objective of this paper.

We have structured the paper as follows: In Sec. II we present a brief overview of the method together with the details of the calculations. We present and discuss the results on Sec. III, and the conclusions are presented in Sec. IV.

II. METHOD AND DETAILS OF THE CALCULATIONS

The optical spectrum of the defect center formed when some Co^{2+} ions substitute for some Zn^{2+} ions in the $KZnF_3$ lattice corresponds to transitions localized in the unit $(CoF_6)^{4-}$, and is supposed to be governed by bonding interactions between the impurity Co^{2+} ion and its first F^- neighbors. These interactions can be adequately described by applying standard high quality quantum mechanical methods to the $(CoF_6)^{4-}$ cluster. These have been Complete Active Space SCF (CASSCF) (Ref. 19) and Average Coupled-Pair Functional (ACPF) (Ref. 20) calculations which include dynamic electron correlation. We have included relativistic effects in the calculations through the use of the Wood-Boring[21]-based effective core potential two-component relativistic Hamiltonian WB-AIMP.[18,22] In order to include simultaneously the effects of electron correlation and spin-orbit coupling, we have used the spin-free-state-shifted Hamiltonian (sfss).[18,23] The details of the $(CoF_6)^{4-}$ cluster calculations are reported in Sec. II B.

The embedding effect due to interactions with the rest of the components of the $KZnF_3$ host lattice is also important. We model it by using the *ab initio* model potential embedding technique.[18,24,25] The details of the embedding model potentials are described in Sec. II A. The calculations have been performed with the MOLCAS-5 package[26] and with a modified version of the COLUMBUS package.[27]

A. Embedding potential

The AIMP embedding technique used here is a practical implementation to the study of local properties of imperfect solids of the group function theory developed by McWeeny,[28] in the context of intermolecular interactions, and Huzinaga,[29] in the context of a core/valence partition. It was presented in Refs. 24 and 30 as a technique to perform calculations on perfect, unpolarized ionic lattices, and later extended[25] to allow for calculations with a relaxed and polarized lattice, represented by a shell-model description.[31] Its application to impurity defects was reviewed in Ref. 18. In practice, the one-electron terms of an isolated cluster hamiltonian are corrected by adding the embedding potential

$$\sum_{\mu} [V_{\mu}^{lr-Coul}(i) + V_{\mu}^{sr-Coul}(i) + V_{\mu}^{exch}(i) + P_{\mu}(i)], \quad (1)$$

where μ runs over the crystal ions (K^+, Zn^{2+}, F^-), $V_{\mu}^{lr-Coul}(i)$ stands for the long-range Coulomb potential exerted by ion μ on the i-th electron of the cluster [i.e., $\Sigma_{\mu} V_{\mu}^{lr-Coul}(i)$ is the Madelung potential of the lattice], $V_{\mu}^{sr-Coul}(i)$ stands for the potential that represents the deviation from point-charge character of the lattice ion (the short-range Coulomb potential), $V_{\mu}^{exch}(i)$ is the exchange potential and $P_{\mu}(i)$ is the orthogonality potential, that prevents the cluster wave function from collapsing into the lattice ion μ. Only the dynamical cluster/lattice correlation is excluded from the embedding potential. The detailed form of these potentials can be found in Refs. 24 and 30, together with the procedure that leads to their calculation from the lattice ions wave functions. In this work, the total-ion potentials just described have been taken from Ref. 14. We refer to this paper for details about its obtention.

The whole AIMP embedding potential is built up by adding the AIMP total-ion potentials of all the lattice ions outside the cluster to the cluster Hamiltonian. The infinite sum is truncated as follows: We include the AIMP embedding potentials of all ions located within a cube of length $3a$ centered in the impurity site ($a = 4.054$ Å), plus all ions located outside this cube but inside the cube of length $6a$; these are point charges bearing the nominal ion charge, except those located at the frontier, that bear fractional charges according to Evjen's method.[32] In this way we can be sure that the cluster embedding potential provides a good representation of the quantum effects as well as the long-range Madelung effects.

As stated above, the AIMP embedding method has been extended to include the polarization and relaxation of the lattice, represented by shell-model potentials, configuring the so-called AIMP/SM method. This end is achieved by a series of iterative calculations of (a) the ground-state potential energy surface of the cluster embedded in a representation of the lattice and (b) the relaxation and distortion of this embedding lattice. To perform the calculations, shell-model parameters and pair potentials are necessary. In this work we have used the same set of parameters used in Ref. 14. The lattice has been relaxed with respect to the electronic ground state a^4T_{1g}. The calculations performed using this relaxed lattice configuration are referred to as AIMP/SM calculations.

B. $(CoF_6)^{4-}$ defect cluster calculations

The calculations on the embedded cluster used a Cowan-Griffin relativistic effective core potential both for Co and F ions. For Co, we used a [Mg]-core CG-AIMP taken from Ref. 33 together with the corresponding $(9s5p5d)$ basis set, augmented with one p polarization function,[34] one d diffuse function,[35] and three f-type functions,[36] finally contracted as $[4s4p5d1f]$. For F, we have used a [He]-core CG-AIMP and the $(5s5p)$ valence basis set of Ref. 33, augmented with a diffuse p-function for the anion[37] and contracted as $[2s3p]$. Following Ref. 38 we have used extra orthogonalization functions for the (100)-second neighbor Zn^{2+} ions, as done in Ref. 14 on $(VF_6)^{4-}$:$KZnF_3$ calculations. These functions are the $(11s8p)$ basis set used for Zn^{2+} on the Zn^{2+}: $KZnF_3$ embedded ion calculations,[14] totally contracted as $[1s1p]$. The total number of basis set functions is 138.

We performed relativistic calculations using the spin-free and spin-orbit hamiltonians for $(CoF_6)^{4-}$ embedded in the AIMP representation of the $KZnF_3$ lattice described above.

TABLE I. Optimized geometries and vibrational frequencies of the $(CoF_6)^{4-}$ cluster. For comparison, $R_0(Zn-F)$ in undoped $KZnF_3$ is 2.027 Å. Distortions with respect to the ground state, $[R_0-R_0(a^4T_{1g})$, AIMP/SM level] are also included for the different electronic states. Results corresponding to spin-free calculations.

	R_0(Co−F)(Å)		$R_0-R_0(a^4T_{1g})$(pm)		$\bar{\nu}_{a_{1g}}$(cm^{-1})	
Electronic state	AIMP	AIMP/SM	This work	Estimated[a]	AIMP	AIMP/SM
a^4T_{1g}	2.067	2.080			519	502
$^4T_{2g}$	2.085	2.099	1.9	3.7	534	518
$^4A_{2g}$	2.101	2.115	3.5	7.7	547	530
a^2E_g	2.047	2.060	−2.0	3.8	498	484
a^2T_{1g}	2.068	2.081	0.1	0.2	516	501
a^2T_{2g}	2.067	2.080	0.0	0.3	515	500
b^4T_{1g}	2.082	2.096	1.6	3.3	533	516
$^2A_{1g}$	2.084	2.098	1.8	3.7	534	518
b^2T_{1g}	2.070	2.083	0.3	0.4	518	503
b^2T_{2g}	2.080	2.093	1.3	4.5	533	515
c^2T_{1g}	2.082	2.095	1.5	2.8	534	518
b^2E_g	2.084	2.098	1.8	3.9	534	517

[a]Estimated using the values of Ref. 9 and our value for $\bar{\nu}_{a_{1g}}(a^4T_{1g})$.

First, we performed complete active space self consistent field (CASSCF)[19] calculations, including seven active electrons in the mainly Co^{2+} $3d$ molecular orbitals. In a second step, we took the whole CASSCF configuration space as a reference for average coupled pair functional (ACPF) (Ref. 20) calculations, aimed to include dynamic correlation effects. These are multireference configuration interaction-singles and doubles calculations with an approximate correction for size-consistency. In these calculations, we correlate the $3d$ and $3p$ metal electrons but only a limited subset of F^- ligand $2p$ electrons, due to computational limitations. These are the electrons that occupy the t_{2g} and e_g F$-2p$ molecular orbitals, ten in total. The use of this type of partitioning of the ligand orbitals was proposed by Pierloot and Vanquickenborne,[39] and provided very good results for geometrical and spectral calculations of transition metal impurity ions with low oxidation states.[18] The total number of electrons correlated is 23. The results of these calculations are presented in the following Tables under the heading ''spin-free'' calculations. We have studied the following spin-free states of the cluster (in parenthesis, we refer the parent free-ion state): the ground state $a^4T_{1g}(^4F)$ and the excited states $^4T_{2g}(^4F)$, $^4A_{2g}(^4F)$, $a^2E_g(^2G)$, $a^2T_{1g}(^2G)$, $a^2T_{2g}(^2G)$, $b^4T_{1g}(^4P)$, $^2A_{1g}(^2G)$, $b^2T_{1g}(^2H)$, $b^2T_{2g}(^2H)$, $c^2T_{1g}(^2H)$, and $b^2E_g(^2H)$. The results of the ACPF calculations have been corrected to take into account the atomic correlation, by computing the free-ion transition energies between the different atomic multiplets at the same level of theory [i.e., correlating 13 electrons of Co^{2+} ($3d$, $3p$) in ACPF calculations]. The difference between these values and the experimental ones is transferred to the cluster calculations. The corrections are 961 cm^{-1} for the $^4F \rightarrow {}^4P$ transition, 1242 cm^{-1} for the $^4F \rightarrow {}^2G$ transition and 2383 cm^{-1} for the $^4F \rightarrow {}^2H$ transition.

The calculations equivalent to these ACPF-23 calculations using the spin-orbit relativistic Hamiltonian are very demanding. As a simpler alternative, we have used in this work the spin-free-state-shifted spin-orbit Hamiltonian (sfss). This Hamiltonian has been described in detail in Refs. 18 and 23 and we refer to those papers for a detailed form of the operators. In a few words, the sfss Hamiltonian results from adding, to the many-electron spin-orbit Hamiltonian, a term that shifts the spin-free states calculated in a small CI space (appropriate to describe the spin-orbit coupling, called the *P* space) to the positions of the same spin-free states calculated in a larger CI space (appropriate to describe dynamic correlation effects, called the *G* space). In this case, the *G* space is the ACPF-23 space described above and the *P* space is defined by the CASSCF reference ($3d$) plus all the single excitations from the main character Co-$3d$ orbitals to the virtual orbitals. This CI calculations have been fed with orbitals optimized for the $^4A_{2g}$ state. The sfss Hamiltonian has been shown to be a very efficient way to include both correlation and spin-orbit effects in an *ab initio* calculation when they can be largely decoupled. Examples can be found for transition-metal elements,[23,40,41] lanthanide elements,[42] and actinide elements.[43] These calculations are referred in the Tables as ''spin-orbit'' calculations.

III. RESULTS AND DISCUSSION

A. Cluster geometries

In Table I we present the results of the geometry optimization of the $(CoF_6)^{4-}$ cluster in different electronic states performed at the spin-free ACPF-23 level, both with a perfect unrelaxed lattice (AIMP) and with a lattice relaxed and polarized consistently with the a^4T_{1g} ground state (AIMP/SM). We optimized the Co-F distance of the $(CoF_6)^{4-}$ unit restricted to O_h symmetry R_0, and calculated the breathing mode vibrational frequencies $\bar{\nu}_{a_{1g}}$ for a number of low-lying electronic states of the cluster. The potential energy surfaces calculated at this spin-free level are represented in Fig. 1. We can see that the Co-F distance is, for all states, larger than the Zn-F distance in the perfect lattice, 2.027 Å, consistent with the slightly larger ionic radius of Co^{2+} compared to Zn^{2+}.[44] The effect of lattice relaxation is an enhancement of the distortion with respect to the perfect lattice situation i.e., the equilibrium distances determined at the AIMP/SM level are larger than the AIMP ones, by 0.013–0.014 Å for all the states. This enhancement represents a 25–30 % of the distortion at the AIMP level for most of the electronic states studied here, in line with other, similar, systems studied before.[14,25,45] On the other hand, the bond distance offsets of the different excited states with respect to the ground state are not significantly affected by lattice relaxation, as can be seen in Table I.

Focusing on the AIMP/SM results, we can see that the equilibrium distances for the different states are grouped depending on the different occupation of the mainly e_g and t_{2g} $3d$ metal orbitals in the leading configurations of each state.

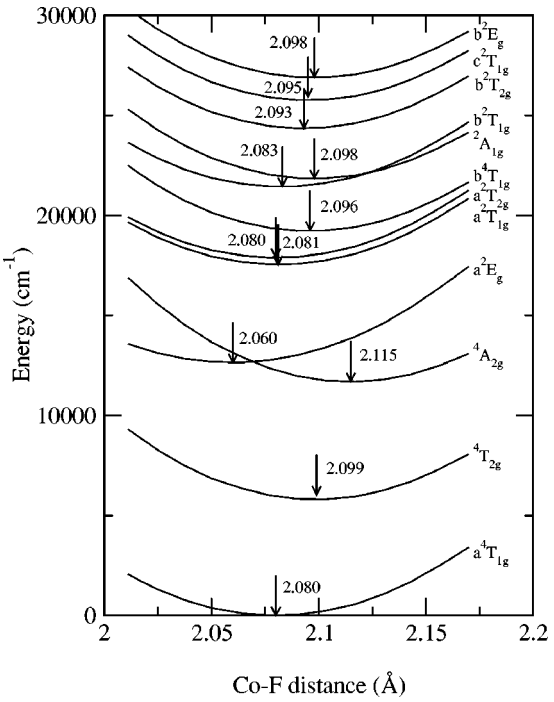

FIG. 1. Potential energy curves of the ground and lowest excited states of the $(CoF_6)^{4-}$ cluster as a function of the Co-F distance in the a_{1g} vibrational mode. The results correspond to spin-free AIMP/SM calculations.

The ground state a^4T_{1g} and the a^2T_{1g}, a^2T_{2g}, and b^2T_{1g} excited states, all corresponding to a $t_{2g}^5e_g^2$ configuration, have a similar equilibrium distance. The states belonging to the $t_{2g}^4e_g^3$ configuration ($^4T_{2g}$, b^4T_{1g}, $^2A_{1g}$, b^2T_{2g}, c^2T_{1g}, and b^2E_g) also have a similar distance, larger than the corresponding to the $t_{2g}^5e_g^2$ configuration, due to the larger occupation of the nonbonding e_g orbitals. Similarly, the $^4A_{2g}$ state ($t_{2g}^3e_g^4$ configuration) has an even larger Co-F distance. Only the a^2E_g state ($t_{2g}^6e_g^1$ configuration) has a smaller equilibrium distance than the ground state, due to the total occupation of the t_{2g} orbitals. It is worth noting here that, in spite of the highly correlated wave function used, the (strong-field) configuration remains an adequate label for the states.

To our knowledge, no direct measurement of these equilibrium distances exists for this material. However, the very good agreement with existing experimental findings obtained by AIMP calculations in similar systems gives credit to our calculated distortions. Indirect estimations of the difference between the equilibrium distance of the different excited states and the ground state can be done using the values for the Huang-Rhys coupling factors (S_e) obtained, using the single-configuration coordinate model, for the different excited states from absorption spectroscopy.[9] Instead of S_e, only the product $S_e\overline{\nu}$ is available from Ref. 9. It is worth noting that these numbers, obtained from the position of broad bands in the absorption spectrum should have relatively large uncertainties. The vibrational energy of the a_{1g} mode is not known, and a number of different vibrational energies are determined from the spectra but they are not assigned to actual vibrational modes. In these circumstances, a different value (223 cm^{-1}, the weighted average energy of the phonon density of states of $KZnF_3$) is used for the determination of S_e. Using it, a value of 2.6 is obtained for the $a^4T_{1g}\rightarrow{}^4T_{2g}$ absorption transition.[9] As a comparison, a value of 4 is given for this factor in Ref. 7, estimated from relative intensity of the zero-phonon transition and the phonon sideband.

On the other hand, using the values of Table III of Ref. 9, our calculated value for $\overline{\nu}_{a_{1g}}$ (502 cm^{-1}, see below) and the formulas quoted by Al-Abdalla *et al.*,[46] we arrived to the estimated distortions shown in Table I, to be compared with our calculated distortions, also shown in the table. We can see that the estimated distortions are very large, a fact that reflects the crude approximations used to obtain the parameters from the experimental information. We will refer later to the quality of our calculated bond distance offsets.

Using the value of 223 cm^{-1} as the enabling frequency, we obtained even larger values for the distortions with respect to the ground state. However, these results are apparently used to build the energy-level diagram for distortions with respect to the a_{1g} vibrational mode for Co^{2+}:$KZnF_3$.[9] This diagram was used in Ref. 9 to interpret the spectroscopic results. Moreover, from the SCC analysis, only the magnitude of the distortions can be obtained but not its sign. In Ref. 9, *all* the distortions are taken to be positive (i.e., the equilibrium distance is larger for the state in question than for the ground state), in contrast with our calculation of a negative distortion for the $a^2E_g(t_{2g}^6e_g^1)$ state. As stated above, the sign of our calculated distortion is consistent with the change in configuration between the two states. As a consequence, we believe that the distortions used to build the SCC diagram are, in view of our calculation, too large, and the sign is erroneous for the $a^2E_g(t_{2g}^6e_g^1)$ state, so that great caution should be taken when using it to interpret the different electronic spectra.

In Fig. 2 we present the energy curves analogous to the ones in Table I and Fig. 1, but calculated at the spin-orbit level. From Fig. 2 we can see that the equilibrium distances are very close to the ones obtained for the related spin-free levels, the difference always being less than 0.005 Å. Thus, in the following, we will calculate the different spectra at the spin-free bond distances found for the different electronic states.

The vibrational energies for the a_{1g} mode are also included in Table I. We can see that these vibrational energies are grouped in the same way as the bond distances, related to the leading electronic configuration. The lattice relaxation slightly decreases the values, the final numbers being 502 cm^{-1} for the a^4T_{1g} ground state. Spin-orbit coupling does not affect these numbers. Again, experimental results are lacking for these vibrational energies, to our knowledge. As cited above, an analysis of the absorption and emission spectra of Co^{2+}:$KZnF_3$[9] gives rise to a number of different phonon energies, but they are not assigned to any vibrational mode, so comparison is not possible. Vibrational modes with frequencies around 500 cm^{-1} are detected in the reflectance spectra of $KCoF_3$ (518 cm^{-1}) and $KZnF_3$(500 cm^{-1}).[47]

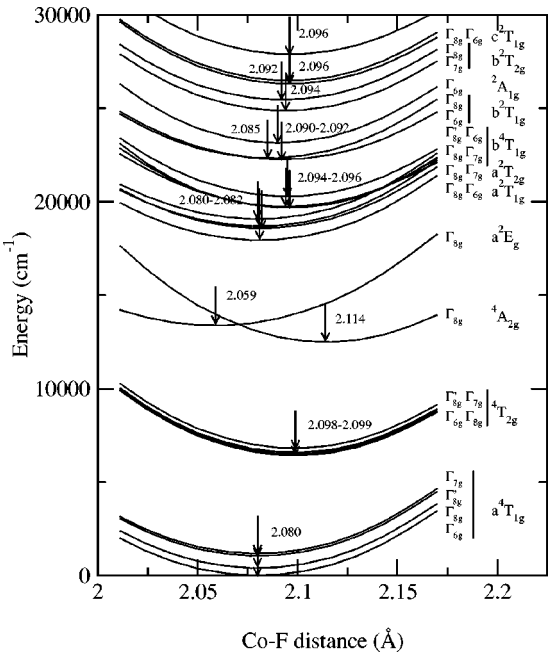

FIG. 2. Potential energy curves of the ground and lowest excited states of the $(CoF_6)^{4-}$ cluster as a function of the Co-F distance in the a_{1g} vibrational mode. The results correspond to spin-orbit AIMP/SM calculations.

Nondegenerate electronic states in cubic environments are Jahn-Teller (JT) unstable, and the coupling with nontotally symmetric vibrational modes removes their degeneracy. As this effect can be important for the interpretation of the electronic spectra (especially, the ESA spectrum) we have reoptimized the geometry of the cluster in the different quartet states involved (a^4T_{1g}, $^4T_{2g}$, b^4T_{1g}). Taking the O_h equilibrium geometry and the embedded-cluster energy as the origin, we have calculated the Jahn-Teller coupling of the different electronic states with the doubly degenerate e_g vibrational mode of the $(CoF_6)^{4-}$ cluster ($T\otimes e$ coupling). We have searched for minima with respect to the $e_{g,\theta}$ normal coordinate, that leads to tetragonal (D_{4h} symmetry) compressed/elongated geometries[48] (neglecting the coupling with triply degenerate t_{2g} modes[49]). The minimization has been performed at the spin-free level (ACPF-23) with the relaxed lattice configuration described above. The results of the calculations are shown in Table II. In this table we present the optimized geometries and the $e_{g,\theta}$ vibrational frequency ($\overline{\nu}_{e_{g,\theta}}$) for both the compressed and elongated structures together with the Jahn-Teller stabilization energy (E_{JT}), the $E_{JT}/\overline{\nu}_{e_{g,\theta}}$ ratio for the most stable state (this last number is a measure of the strong/weak linear JT coupling[48]), and the ratio $\overline{\nu}_{e_{g,\theta}}/|2\beta|$ (where 2β is the energy difference between the elongated and compressed structures) which is a measure of static/dynamic behavior in the limit of strong JT coupling.

The results show quite different JT couplings for the three states. The a^4T_{1g} ground state shows a very small distortion, totally negligible in terms of energy, with just an $8-\text{cm}^{-1}$ stabilization. The $^4T_{2g}$ state has a weak linear coupling, the singly degenerate $^4B_{2g}$ being the most stable state, in an elongated structure. The Jahn-Teller stabilization energy (E_{JT}) for this state is 120 cm^{-1}. The Jahn-Teller effect can be characterized as dynamic in this case. The b^4T_{1g} state, on the other side, exhibits a fairly strong coupling, giving rise to a static Jahn-Teller effect ($\overline{\nu}_{e_{g,\theta}}/|2\beta|$ is almost equal to unity), the distortion being a compression in this case. E_{JT} is 545 cm^{-1} in this case. The vibrational frequency $\overline{\nu}_{e_{g,\theta}}$ is, for the three states, of some 400 cm^{-1}.

TABLE II. Equilibrium tetragonal geometries and Jahn-Teller $T\otimes e$ coupling parameters for the a^4T_{1g}, $^4T_{2g}$, and b^4T_{1g} electronic states.

	a^4T_{1g}	$^4T_{2g}$	b^4T_{1g}
Octahedral structure			
R_0 (Co-F) (Å)	2.080	2.099	2.096
$\overline{\nu}_{a_{1g}}$ (cm^{-1})	502	518	516
Elongated D_{4h} structure	$^4A_{2g}$	$^4B_{2g}$	^4E_g
R_{ax} (Co-F) (Å)	2.090	2.129	2.127
R_{eq} (Co-F) (Å)	2.075	2.083	2.081
$\overline{\nu}_{e_{g,\theta}}$(cm^{-1})	402	399	419
E_{JT} (cm^{-1})	8	120	
$E_{JT}/\overline{\nu}_{e_{g,\theta}}$	0.02	0.30	
2β(cm^{-1})	8	93	
$\overline{\nu}_{e_{g,\theta}}/\|2\beta\|$	50.3	4.3	
Compressed D_{4h} structure	^4E_g	^4E_g	$^4A_{2g}$
R_{ax} (Co-F) (Å)	2.075	2.083	2.035
R_{eq} (Co-F) (Å)	2.083	2.107	2.127
$\overline{\nu}_{e_{g,\theta}}$ (cm^{-1})	395	396	420
E_{JT} (cm^{-1})			545
$E_{JT}/\overline{\nu}_{e_{g,\theta}}$			1.30
2β (cm^{-1})			415
$\overline{\nu}_{e_{g,\theta}}/\|2\beta\|$			1.0

To our knowledge, there are no experimental measurements of these distortions in any of the states. From a study of the Ham quenching of the spin-orbit levels in the $^4T_{2g}$ state in the related system Co^{2+}: $KMgF_3$, a value of around 500 cm^{-1} for E_{JT} is suggested for this state.[49] We expect the values of E_{JT} for this state to be similar in both hosts, $KZnF_3$ and $KMgF_3$ (see Ref. 15). Although the Jahn-Teller effect is considered as dynamic in both studies (in our study, the coupling is weak; in the experimental study, the coupling is stronger, but the ratio between the vibrational frequency and the energy barrier agrees with a dynamical behavior), our calculated value is much smaller than experimentally suggested. Such discrepancies are usual in the determination of these parameters (see, for example, Refs. 11 and 15) as well as between different experimental estimations, due to the approximations used in the fittings. As a matter of fact, the value suggested for E_{JT} in Ref. 49 is obtained from a crystal-field calculation of the splitting of the spin-orbit levels of the $^4T_{2g}$ state against the parameter $3E_{JT}/\overline{\nu}_{e_{g,\theta}}$. From it, the optimum value of $E_{JT}/\overline{\nu}_{e_{g,\theta}}$ is obtained. In this case, the best fit takes place in the zone of a small slope of the curves,

leading to a large uncertainty in the determination of $E_{JT}/\overline{\nu}_{e_{g,\theta}}$. The value of the splittings is itself very dependent on the parameters used in the crystal-field calculation, especially the spin-orbit coupling constant ζ, and different values for it were reported in different sources.[9,49] We believe that the close agreement found in similar systems[46] between experimental and calculated $e_{g,\theta}$ distortions gives credit to the ones calculated in this work, and to the E_{JT} values obtained, closely related to them.

Some qualitative information can be extracted from a comparison of our studied system with the related V^{2+}-doped $KMgF_3$.[11,50] V^{2+} has an atomic d^3 structure, so their states as an impurity can be related to the holes in the d^7 structure of Co^{2+}. This way, the JT coupling in the b^4T_{1g} state of V^{2+} ($t_{2g}e_g^2$) in $KMgF_3$ is found to be inconsequential for the spectrum, as it is found by us in the related a^4T_{1g} state ($t_{2g}^5e_g^2$), due to the single occupation of both e orbitals. The distortion in the $^4T_{2g}$ and a^4T_{1g} states in V^{2+}, both coming from the same $t_{2g}^2e_g$ configuration, is estimated to be of opposite sign (i.e., one is elongated, the other compressed),[11] as we calculate for the $^4T_{2g}$ and b^4T_{1g} states of Co^{2+}. However, in Ref. 11, the coupling is supposed to be the same for both $^4T_{2g}$ and a^4T_{1g} of V^{2+} (i.e., the same values for E_{JT}), but we find quite different values of E_{JT} for both states. Finally, it should be pointed out that no experimental determination of the $e_{g,\theta}$ vibrational frequency exist for Co^{2+}:$KZnF_3$. In Ref. 49, for Co^{2+}: $KMgF_3$, values of $200-300$ cm^{-1} for it are used without further explanation. In reflectance spectra,[47] modes with adequate symmetry are found at 449 cm^{-1} ($KCoF_3$) and 424 cm^{-1} ($KZnF_3$). We have not determined the geometrical parameters for the JT structures at the spin-orbit level.

B. Electronic transitions

The results of the minimum-to-minimum transition energies between the different states at the spin-free and spin-orbit levels, both with a relaxed lattice, are shown in Table III. Zero-phonon transitions should be very close in energy, as vibrational frequencies are very similar for the different electronic states studied here. Together with our calculated values, we present the experimentally observed and estimated positions,[9] obtained from absorption and emission spectra. Other spectra have been found in the literature,[7,10] from which these zero-phonon energies have been determined. The results do not differ from those cited in Ref. 9; in fact, the different lines was assigned in Ref. 10 by a direct comparison with those of Ref. 9. The comparison of our calculated values with the experimental ones is satisfactory, the differences being very small for the first transitions and around 1000 cm^{-1} for the transitions to the b^4T_{1g} and b^2T_{1g} states. It should be pointed out that these later values are only estimated in the experiment,[9] because only band maxima are seen in absorption. These differences are in line with those obtained in previous calculations of low oxidation state transition-metal impurities in solids,[18] and their origin may lie in the insufficient treatment of the dynamic electron correlation. The ordering of the states is the same observed in the experimental spectrum. However, we should notice that the $^4A_{2g}$ lies below the a^2E_g state (see Fig. 2), opposite to the crystal-field calculation quoted in Ref. 9. This result may be related to the above mentioned disagreement in the a^2E_g state offset. From the experimental spectra it is not possible to determine the relative position of these two states. In absorption spectrum, only a small shoulder starting around 12 500 cm^{-1} (at 300 K) can be seen,[9] attributed to the $a^4T_{1g}\rightarrow{}^4A_{2g}$ absorption, but its exact position cannot be determined. In the absorption spectrum of Ref. 7, obtained after electron irradiation of the material, a band, visible although not very intense, can be seen starting around 11 000 cm^{-1} (a maximum around 12 000 cm^{-1}) and it is not assigned by the authors. We think that these bands correspond to the $a^4T_{1g}\rightarrow{}^4A_{2g}$ transition, and that it should be flanked on its high energy side by the $a^4T_{1g}\rightarrow a^2E_g$ transition.

The spin-orbit splitting calculated by us results to be around 10% larger than the experimentally determined for the ground state. It is also larger for the $^4T_{2g}$ state, although for this state the Ham effect[51] should reduce the spin-orbit splitting, and we do not consider this effect in our calculations [incidentally, the splitting calculated by us for this state agrees almost quantitatively with the one calculated in Ref.

TABLE III. Minimum-to-minimum transitions between different electronic states. All numbers in cm^{-1}.

Spin free		Spin orbit		
State	Energy	State	Energy	Experiment [a]
a^4T_{1g}	0	Γ_{6g}	0	0
		Γ_{8g}	395	293
		Γ'_{8g}	1045	940
		Γ_{7g}	1170	
$^4T_{2g}$	5800	Γ_{6g}	6420	6595
		Γ_{8g}	6490	6603
		Γ'_{8g}	6580	6675
		Γ_{7g}	6810	
$^4A_{2g}$	11680	Γ_{8g}	12485	
a^2E_g	12645	Γ_{8g}	13375	
a^2T_{1g}	17550	Γ_{8g}	17940	
		Γ_{6g}	18585	
a^2T_{2g}	17885	Γ_{8g}	18690	
		Γ_{7g}	19075	
b^4T_{1g}	19215	Γ_{8g}	19680	(18700)
		Γ_{7g}	19680	
		Γ'_{8g}	19725	
		Γ_{6g}	20280	(19750)
b^2T_{1g}	21435	Γ_{6g}	22260	(21350)
		Γ_{6g}	22335	
$^2A_{1g}$	21845	Γ_{6g}	23150	
b^2T_{2g}	24350	Γ_{7g}	24865	
		Γ_{8g}	25460	
c^2T_{1g}	25755	Γ_{6g}	26310	
		Γ_{8g}	26475	
b^2E_g	26885	Γ_{8g}	27890	

[a]Values measured or estimated (in parentheses), taken from Ref. 9.

49 using crystal-field theory at a zero Jahn-Teller coupling, for the related system Co^{2+}: $KMgF_3$ (see Fig. 6 in Ref. 49). This quantitative agreement should be mainly fortuitous]. The Jahn-Teller coupling is insignificant in the a^4T_{1g} ground state, so no Ham quenching is expected. For the b^4T_{1g} excited state, on the other side, the Jahn-Teller effect is predicted to be rather static and the Ham effect should not then be present. In fact, for this state we predict a smaller splitting than that experimentally estimated, although experimental data are not as reliable in this case as for the other bands.

The good agreement of the calculated spectrum with the experimental one gives credit to our determined bond distance offsets of the different electronic states. We have made a further check by calculating the band shape of an emission band. This band shape is essentially controlled by the a_{1g} vibrational mode offset and frequency and, provided the latter is of good quality, a good reproduction of the band shape would validate the former. To calculate this band shape, we have used the semiclassical time dependent approach of Heller.[52,53] In Fig. 3 we present the band shape of the emission from the $\Gamma'_{8g}(^4T_{2g})$ state to the $\Gamma_{6g}(a^4T_{1g})$ state, calculated using the values of the offset obtained by us (0.019 Å, thin solid line) and those derived from the values of Ref. 9 (0.037 Å, thin dashed line), both using $\overline{\nu}_{a_{1g}}=502\ \mathrm{cm}^{-1}$ (see Table I). For comparison, we have plotted also the experimental profile of the emission, taken directly from Fig. 5 of Ref. 9, shifted in energy. We have scaled the calculated band shape so that the intensity of the second peak (around 6100 cm^{-1}) coincides in the three lines. From the figure we can see that the overall agreement of the band shape calculated using our bond-distance offset with the experimental data is very satisfactory, taking into account the complexity of the emission band [with several different electronic origins; for example, at around 5600 cm^{-1}, our calculated band seems to be overlapped with the origin of the $\Gamma'_{8g}(^4T_{2g}) \rightarrow \Gamma'_{8g}(a^4T_{1g})$ emission]. On the other hand, the shape of the emission band calculated with the offset derived from the values of Ref. 9 is in complete disagreement with the experimental band. In our opinion, the results contained in Fig. 3 validate the bond-distance offsets calculated in this work.

We will comment now on the excited state absorption spectrum. This ESA spectrum has been measured,[9] between 28 500 and 6900 cm^{-1}, after exciting the sample of Co^{2+}:$KZnF_3$ into the b^4T_{1g} excited state using a laser at 532 nm (18 800 cm^{-1}). As can be seen in Fig. 10 of Ref. 9, the spectrum consists of two broad bands, one with the maximum at 8000 cm^{-1}, and the second one peaking at 12 350 cm^{-1}. This second band has a shoulder clearly indicating that this band is composed of two different bands, the second of them with the maximum at around 13 350 cm^{-1}. Both bands are supposed to be related to transitions from the first excited quartet state, $^4T_{2g}$. Using the SCC model (whose reliability we commented above) and the fact that only transitions between states of the same spin should have a reasonable intensity, the two broad (excited-state) absorptions are assigned[9] to the $^4T_{2g} \rightarrow {}^4A_{2g}$ and $^4T_{2g} \rightarrow b^4T_{1g}$ transitions, respectively. Based on the main electronic configuration of each state ($t_{2g}^4e_g^3$ for $^4T_{2g}$ and b^4T_{1g}, $t_{2g}^3e_g^4$ for $^4A_{2g}$), the bands are predicted to be broad and narrow, respectively. In view of these results, the second band is not assigned solely to the $^4T_{2g} \rightarrow b^4T_{1g}$ transition. Two hypothesis are discussed to explain the width of this second band: (1) a strong JT effect in any of the two states involved or (2) a "tunneling effect" between the b^4T_{1g}, a^2T_{1g}, and a^2T_{2g} states.[9] By making an analysis of the JT coupling based on the work by Payne *et al.*[11] on V^{2+}: $KMgF_3$, and using a value of E_{JT} of 500 cm^{-1},[49] the authors concluded that the first reason can not explain the position and width of the band. The two bands were assigned then to the $^4T_{2g} \rightarrow {}^4A_{2g}$ transition (around 8000 cm^{-1}) and to the $^4T_{2g} \rightarrow b^4T_{1g}$ transition (around 13 350 cm^{-1}), broadened by spin-orbit mixing with the a^2T_{1g} and a^2T_{2g} states. In view of our calculations, we do not agree with these assignments, at least partially.

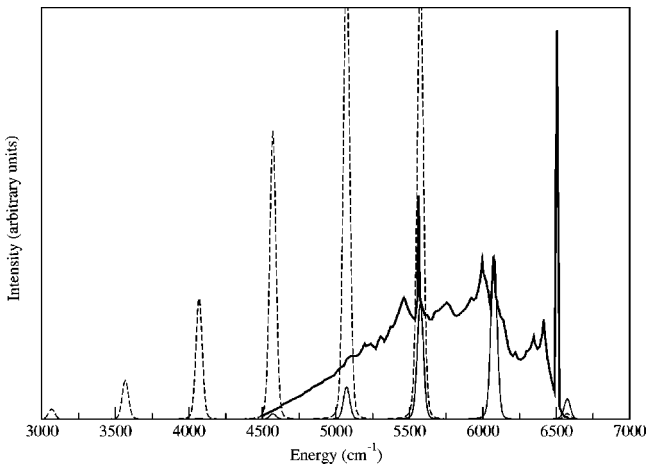

FIG. 3. Intensity profile of the emission band from the $\Gamma'_{8g}(^4T_{2g})$ state to the $\Gamma_{6g}(a^4T_{1g})$ state. Thin solid line: present calculation. Thin dashed line: calculation with offset estimated using results from Ref. 9. Thick line: experimental emission spectrum, taken from Fig. 5 of Ref. 9 (shifted in energy).

The ESA spectrum, calculated as the vertical transitions from the minimum of the $^4T_{2g}$ electronic state energy curve (or from the Γ_{6g} spin-orbit component, in the spin-orbit calculations), is shown in Table IV. Starting with the second band, we indeed see from this table that the $^4T_{2g} \rightarrow b^4T_{1g}$ transition is located around 13 400 cm^{-1}, and is split by spin-orbit interaction by some 600 cm^{-1}. Transitions to the a^2T_{1g} and a^2T_{2g} states are calculated at 11 870 and 12 220 cm^{-1}, respectively. However, the very strong spin-orbit mixing necessary to explain the experimental peak at around 12 350 cm^{-1} cannot be explained from our calculations, as the contribution of the spin-free b^4T_{1g} state to the wave function of the different spin-orbit components of a^2T_{1g} and a^2T_{2g} states is almost negligible (less than 0.5% in all cases). It is also difficult to explain the fact that it is the peak at lower energy (12 350 cm^{-1}) the one that carries the more intensity, being spin forbidden (to first order at least). Taking these facts into account, we have decided to try to validate the first hypothesis (i.e., the Jahn-Teller coupling) as being responsible for the bandwidth. To this end, we have calculated the vertical electronic transitions from the mini-

TABLE IV. Vertical excited state absorptions from the minimum of the $^4T_{2g}$ state, O_h symmetry. All numbers in cm^{-1}.

Spin free		Spin orbit	
State	Energy	State	Energy
$^4T_{2g}$	0	Γ_{6g}	0
		Γ_{8g}	70
		Γ'_{8g}	160
		Γ_{7g}	390
$^4A_{2g}$	6000	Γ_{8g}	6185
a^2E_g	7440	Γ_{8g}	7550
a^2T_{1g}	11870	Γ_{8g}	11645
		Γ_{6g}	12275
a^2T_{2g}	12220	Γ_{8g}	12395
		Γ_{7g}	12790
b^4T_{1g}	13415	Γ_{8g}	13260
		Γ_{7g}	13265
		Γ'_{8g}	13315
		Γ_{6g}	13870
b^2T_{1g}	15740	Γ_{6g}	15858
		Γ_{8g}	15990
$^2A_{1g}$	16040	Γ_{6g}	16760

TABLE V. Vertical excited state absorptions from the minimum of the $^4T_{2g}$ state, D_{4h} symmetry. All numbers in cm^{-1}.

Spin-free			Spin orbit	
O_h	D_{4h}	Energy	D_{4h}	Energy
$^4T_{2g}$	$^4B_{2g}$	0	Γ_{6g}	0
	^4E_g	370	Γ_{7g}	100
			Γ_{6g}	270
			Γ_{6g}	355
			Γ_{7g}	440
			Γ_{7g}	660
$^4A_{2g}$	$^4B_{1g}$	6265	Γ_{6g}	6360
			Γ_{7g}	6360
a^2E_g	$^2A_{1g}$	7330	Γ_{6g}	7360
	$^2B_{1g}$	8085	Γ_{7g}	8110
a^2T_{1g}	^2E_g	11915	Γ_{6g}	11715
	$^2A_{2g}$	12310	Γ_{7g}	11815
			Γ_{6g}	12480
a^2T_{2g}	$^2B_{2g}$	12445	Γ_{7g}	12540
	^2E_g	12600	Γ_{7g}	12745
			Γ_{6g}	12845
b^4T_{1g}	^4E_g	13405	Γ_{7g}	13165
	$^4A_{2g}$	14210	Γ_{7g}	13195
			Γ_{6g}	13235
			Γ_{6g}	13460
			Γ_{7g}	13970
			Γ_{6g}	14290
b^2T_{1g}	$^2A_{2g}$	15910	Γ_{7g}	15960
	^2E_g	15980	Γ_{6g}	15980
			Γ_{6g}	16260
$^2A_{1g}$	$^2A_{1g}$	16305	Γ_{6g}	16920

mum of the elongated D_{4h} structure ($^4B_{2g}$ state), resulting from the $T\otimes e$ coupling of the $^4T_{2g}$ state (see Table II), to the different electronic states. The results of these calculations, both at the spin-free and spin-orbit levels, are presented in Table V. (Note that, at the spin-orbit level, all the states in D_{4h} symmetry belong the Γ_{6g} and Γ_{7g} irreps of the double group, being nondegenerate).

As stated above, the hypothesis of JT coupling as responsible for the width of this band was ruled out by the authors in Ref. 9 by following the analysis of Payne.[11] In it, the JT coupling was considered to be of the same magnitude in both states, $^4T_{2g}$ and b^4T_{1g}. However, we can see in Table II that the coupling is much larger for the b^4T_{1g} state than for the $^4T_{2g}$ state (E_{JT} 545 vs 120 cm^{-1}, respectively). Due to this fact, we find, in D_{4h} symmetry (spin-free), two transitions, one to the $^4E_g(b^4T_{1g})$ state, at 13 405 cm^{-1}, approximately the same energy as the original $^4T_{2g}\rightarrow b^4T_{1g}$ transition in O_h symmetry, and a second one to the $^4A_{2g}(b^4T_{1g})$ state at 14 210 cm^{-1}, both broadened by spin-orbit interaction. We believe that this splitting is the origin of the two maxima seen in the experimental spectrum. The existence of a the so-called ''tunneling effect'' with the doublets is not ruled out by the calculations, but it is not necessary in order to explain the double band seen in the experimental spectrum. The positions of the bands are calculated with an error of around 1000 cm^{-1} at the spin-free level and around 700−800 cm^{-1} at the spin-orbit level, in line with the error found in the calculation of the position of the b^4T_{1g} state.

We now focus on the band at 8000 cm^{-1}. As stated above, this band is assigned to the $^4T_{2g}\rightarrow{}^4A_{2g}$ transition[9] using the SCC analysis. Looking at Table V, this transition is calculated by us at around 6300 cm^{-1}. Taking into account the good agreement found with the experiment for the rest of the electronic transitions, this difference (around 1700 cm^{-1}) seems to be too large to be reasonable. Thus, we believe that the transition seen in the ESA spectrum at 8000 cm^{-1} does not correspond the $^4T_{2g}\rightarrow{}^4A_{2g}$ transition. This transition should be seen in the spectrum, in any case, as it corresponds to a spin-allowed transition, with a reasonable intensity. However, according to our calculations, the band should be centered around 6300 cm^{-1}, outside the range of the experimental data shown in Ref. 9 (14 300−7100 cm^{-1}). As this would be the only spin-allowed transition from the $^4T_{2g}$ state present in this energy region, we suppose that the band has a different origin than the $^4T_{2g}$ state. We should remember that the pumping in the experiment was performed into the upper-lying b^4T_{1g} state. A nonradiative decay follows this pumping according to Ref. 9, ending in the$^4T_{2g}$ state, from which the (excited-state) absorption takes place. But we think that transitions from intermediate states can also be possible, giving rise to multiple-excited-state absorptions, as described previously.[16] Thus we proposed an assignment of the band in question, as due to the transition from the $^4A_{2g}$ state to the upper b^4T_{1g} state. To validate this assignment, we have calculated the excited state absorption spectrum from the minimum of the $^4A_{2g}$ ($t_{2g}^3e_g^4$ main configuration), as vertical transitions to the

TABLE VI. Vertical emission and excited state absorption from the $^4A_{2g}$ state. All numbers in cm^{-1}.

Electronic state		Emission		ESA	
		Spin free	Spin orbit	Spin free	Spin orbit
a^4T_{1g}	Γ_{6g}	11165	11975		
	Γ_{8g}		11585		
	Γ'_{8g}		10930		
	Γ_{7g}		10800		
$^4T_{2g}$	Γ_{6g}	5755	5940		
	Γ_{8g}		5870		
	Γ'_{8g}		5785		
	Γ_{7g}		5550		
$^4A_{2g}$	Γ_{8g}	0	0	0	0
a^2E_g	Γ_{8g}			2170	2095
a^2T_{1g}	Γ_{8g}			6340	5940
	Γ_{6g}				6555
a^2T_{2g}	Γ_{8g}			6710	6690
	Γ_{7g}				7090
b^4T_{1g}	Γ_{8g}			7700	7360
	Γ_{7g}				7370
	Γ'_{8g}				7435
	Γ_{6g}				7975
b^2T_{1g}	Γ_{6g}			10195	9995
	Γ_{6g}				10225
$^2A_{1g}$	Γ_{6g}			10295	10960
b^2T_{2g}	Γ_{7g}			12885	12590
	Γ_{8g}				13200
c^2T_{1g}	Γ_{6g}			14245	13990
	Γ_{8g}				14160
b^2E_g	Γ_{8g}			15335	15555

rest of the states. The results of these calculations, at the spin-free and spin-orbit levels, can be seen in Table VI.

Taking into account the spin rules, only the $^4A_{2g} \rightarrow b^4T_{1g}$ absorption is expected to be detected in the spectrum. This transition is calculated at 7700 cm^{-1}, broadened by spin-orbit coupling. This energy matches very well the experimentally found transition; thus, we assigned the band at lower energy in the ESA spectrum to the $^4A_{2g} \rightarrow b^4T_{1g}$ electronic transition. This assignment rests upon the assumption of a certain stability of $^4A_{2g}$, that makes it possible to measure the absorption from it. The population of this state during the experiment comes from the nonradiative decay of the sample pumped at resonance with the $a^4T_{1g} \rightarrow b^4T_{1g}$ absorption (18 800 cm^{-1}). The possibility of a certain population of the $^4A_{2g}$ state after this decay depends on the decay rates from this state to the states that lie close or below it (a^2E_g, $^4T_{2g}$, and a^4T_{1g}), both radiative and nonradiative. The larger these decay rates, the smaller population of this state. Radiative decay rates are related to the absorption cross section of the transition. From the (ground-state) absorption spectrum, we can see that the cross section of the $a^4T_{1g} \rightarrow {}^4A_{2g}$ absorption is small, as the transition implies a two-electron change in the state configuration. Thus the radiative decay rate to the ground state from the $^4A_{2g}$ state should be very small. The transition to the $^4T_{2g}$ state is a one-electron transition, so it should be relatively intense, similar in intensity to the other spin-allowed transitions. The radiative decay rate should then be similar to that of the $^4T_{2g} \rightarrow a^4T_{1g}$ emission. Nonradiative decay rates are given by

$$w_{NR} \propto |M|^2 g(\Omega), \tag{2}$$

where M is the matrix element, between the two states involved, of the operator that connects them and $g(\Omega)$ is the density of vibronic states in the final states.[54] In a first, crude, approximation, this latter factor can be expressed as

$$g(r) = e^{-S} S^r / r!, \tag{3}$$

where S is the Huang-Rhys parameter and r is the number of phonons emitted in the transition, so that $r\nu$ is the energy difference between the states (where ν is the frequency of the accepting vibrational mode). For the transition to the a^2E_g, no operator connects both states ($^4A_{2g}$ and a^2E_g) at least to first order, as the transition involves a three-electron jump. The (nonradiative) decay rate should be negligible then. For the transition to the ground state a^4T_{1g}, again the fact that the transition is a two-electron change makes this electronic factor very small. Moreover, if we consider the a_{1g} vibrational mode as the accepting one, whose frequency we calculate as 502 cm^{-1} (see Table I), r is around 24 for this transition. The nonradiative decay rate to the a^4T_{1g} state should be negligible too. For the transition to the $^4T_{2g}$ state, the spin orbit connects the two states. The value of $|M|$ should be of the same order of magnitude of the value found for the $^4T_{2g} \rightarrow a^4T_{1g}$ emission, also connected by spin-orbit coupling. From the values of Table I we can estimate the value of S for the $^4A_{2g} \rightarrow {}^4T_{2g}$ transition (0.22) and for the $^4T_{2g} \rightarrow a^4T_{1g}$ transition (0.31). We see that S is also similar for both transitions. r is around 11 for both transitions, so the vibronic factor should be very similar in both cases. As the nonradiative decay rates to the other states are negligible, we conclude that the total decay rates for the $^4A_{2g}$ and $^4T_{2g}$ states should be of the same order of magnitude. As the $^4T_{2g}$ state is clearly populated in the pumping process, we think that it is not unreasonable to have some population on the $^4A_{2g}$ state too, so that the ESA can be detected with it as initial state.

If this population process takes place, together with the ESA, emission should be detected from the $^4A_{2g}$ state. However, to our knowledge, no luminiscence has been reported in the literature from the $^4A_{2g}$ state. In Table VI, we present the calculated emission energies from the minimum of the $^4A_{2g}$ state to both $^4T_{2g}$ and a^4T_{1g} states. As stated above, the transition to the a^4T_{1g} ground state implies a two-electron jump, so its intensity should be very small. On the other hand, the emission to the $^4T_{2g}$ state should have an appreciable intensity. Following Table VI, we see that the emission energy, around 5755 cm^{-1}, overlaps the range of the intense $^4T_{2g} \rightarrow a^4T_{1g}$ emission. The $^4A_{2g} \rightarrow {}^4T_{2g}$ transition can be hidden then by the other emission.

These assignments can have some influence in the explanation of the optical properties of the material. In fact, the $^4T_{2g} \rightarrow a^4T_{1g}$ transition in this material has been charac-

terized as a tunable laser.[7–9] The tuning range goes from around 5800 cm^{-1} to around 4600 cm^{-1}, although the zero-phonon transition is located around 6600 cm^{-1}. The laser performance of this Co^{2+}:$KZnF_3$ material is worse than in other related materials like Co^{2+}:MgF_2.[7,9] These facts can be related to the presence of the previously undetected ${}^4T_{2g} \rightarrow {}^4A_{2g}$ ESA, that should be located around 6,300 cm^{-1} and then compete with the laser emission.

On the other hand, the presence of more than one metastable excited state (both ${}^4T_{2g}$ and ${}^4A_{2g}$) makes the material a good candidate to show upconversion luminiscence. In effect, the ${}^4A_{2g}$ state could probably be populated by ESA from the ${}^4T_{2g}$ state, in a typical situation of GSA/ESA upconversion mechanism. However, the upconverted luminiscence should be difficult to detect, because, as commented above, the ${}^4A_{2g} \rightarrow a^4T_{1g}$ emission goes through a two-electron jump. Nor should be visible any luminiscence from the closely lying a^2E_g state, as the nonradiative decay of the ${}^4A_{2g}$ to it should not proceed. Further experimental investigations about these properties could throw some light on the question.

IV. CONCLUSIONS

In this work, we have performed *ab initio* calculations on the geometric structure and electronic spectra of Co^{2+} impurities hosted in $KZnF_3$. We have obtained equilibrium geometries and vibrational frequencies for the totally symmetric a_{1g} mode for a number of electronic states, also taking into account the Jahn-Teller coupling with the e_g modes in some of them. From the minima of the energy curves, we have obtained values for the different transition energies, both minimum-to-minimum and vertical transitions. The agreement found with available experimental data is very good and allows us to perform new assignments of the ESA bands, where the experimental data were misinterpreted before. To sum up, we find that the band found in the ESA spectrum at around 8000 cm^{-1} should be assigned to the ${}^4A_{2g} \rightarrow b^4T_{1g}$ transition, since the ${}^4A_{2g}$ state can be populated after the pumping process and (excited-state) absorption should be expected from it. This band was previously assigned to the ${}^4T_{2g} \rightarrow {}^4A_{2g}$ absorption, but we find this transition to occur at a smaller energy, around 6300 cm^{-1}, overlapping the laser emission (${}^4T_{2g} \rightarrow a^4T_{1g}$). On the second hand, the broad band found at around 12 500 cm^{-1} corresponds to the ${}^4T_{2g} \rightarrow b^4T_{1g}$ absorption, and shows two maxima that are consistent with transitions to the two states in which a strong Jahn-Teller effect splits the b^4T_{1g} state (${}^4E_g$ and ${}^4A_{2g}$, in D_{4h} symmetry).

The calculations reported in this work clearly show that valuable information that complements the experiment can be extracted using high-quality computational methods. Especially in cases where experimental spectral parameters (such as vibrational frequencies, bond-distances offsets, etc.) are not available with high precision, quantum-mechanical calculations may be a very useful source of information.

ACKNOWLEDGMENT

The author gratefully acknowledges Dr. Luis Seijo and Dr. Zoila Barandiarán (UAM, Madrid, Spain) for continuous support and for helpful comments throughout the work as well as for a critical reading of the manuscript. Part of the calculation presented in this work was performed at the facilities of ''*Centro de Computación Científica* (CCC),'' U. Autónoma de Madrid. This work was partly supported by MCyT (Dirección General de Investigación PB98-0108), Spain.

[1] *Tunable Solid-State Lasers*, edited by P. Hammerling, A. B. Budgor, and A. Pinto, Springer Series in Optical Science, vol. 47 (Springer, Berlin, 1985).
[2] *Tunable Solid-State Lasers II*, edited by A. B. Budgor, L. Esterowitz, and L. G. DeShazer, Springer Series in Optical Science, vol. 52 (Springer, Berlin, 1986).
[3] P.F. Moulton and A. Mooradian, Appl. Phys. Lett. **35**, 838 (1979).
[4] U. Brauch and U. Dürr, Opt. Commun. **49**, 61 (1984).
[5] U. Brauch and U. Dürr, Opt. Lett. **9**, 441 (1984).
[6] U. Brauch and U. Dürr, Opt. Commun. **55**, 35 (1985).
[7] W. Künzel, W. Knierim, and U. Dürr, Opt. Commun. **36**, 383 (1981).
[8] K.R. German, U. Dürr, and W. Künzel, Opt. Lett. **11**, 12 (1986).
[9] H. Manaa, Y. Guyot, and R. Moncorgé, Phys. Rev. B **48**, 3633 (1993).
[10] P.T.C. Freire, V. Lemos, O. Pilla, and N.D. Vieira, Jr., J. Chem. Phys. **110**, 3995 (1999).
[11] S.A. Payne, L.L. Chase, and G.D. Wilke, Phys. Rev. B **37**, 998 (1988).
[12] C.W. Struck and W.H. Fonger, J. Lumin. **10**, 1 (1975).
[13] R. Moncorgé and T. Benyattou, Phys. Rev. B **37**, 9177 (1988).
[14] S. López-Moraza, J.L. Pascual, and Z. Barandiarán, J. Chem. Phys. **103**, 2117 (1995).
[15] S. López-Moraza and Z. Barandiarán, J. Chem. Phys. **105**, 50 (1996).
[16] S. López-Moraza, L. Seijo, and Z. Barandiarán, Phys. Rev. B **57**, 11 974 (1998).
[17] S. López-Moraza, L. Seijo, and Z. Barandiarán, Int. J. Quantum Chem. **77**, 961 (2000).
[18] L. Seijo and Z. Barandiarán, in *Computational Chemistry: Reviews of Modern Trends*, edited by J. Leszczynski (World Scientific, Singapore, 1999), vol. 4, p. 55.
[19] B.O. Roos, P.R. Taylor, and P.E.M. Siegbahn, Chem. Phys. **48**, 157 (1980); P.E.M. Siegbahn, A. Heiberg, J. Almlöf, and B.O. Roos, J. Chem. Phys. **74**, 2384 (1981); P. Siegbahn, A. Heiberg, B. Roos, and B. Levy, Phys. Scr. **21**, 323 (1980).
[20] R. Ahlrichs, P. Scharf, and C. Ehrhardt, J. Chem. Phys. **82**, 890 (1985); R.J. Gdanitz and R. Ahlrichs, Chem. Phys. Lett. **143**, 413 (1988).
[21] J.H. Wood and A.M. Boring, Phys. Rev. B **18**, 2701 (1978).
[22] L. Seijo, J. Chem. Phys. **102**, 8078 (1995).
[23] R. Llusar, M. Casarrubios, Z. Barandiarán, and L. Seijo, J. Chem. Phys. **105**, 5321 (1996).

[24] Z. Barandiarán and L. Seijo, J. Chem. Phys. **89**, 5739 (1988).
[25] J.L. Pascual and L. Seijo, J. Chem. Phys. **102**, 5368 (1995).
[26] MOLCAS version 5, K. Andersson, M. Barysz, A. Bernhardsson, M. R. A. Blomberg, D. L. Cooper, T. Fleig, M. P. Fülscher, C. de Graaf, B. A. Hess, G. Karlström, R. Lindh, P.-Å. Malmqvist, P. Neogrády, J. Olsen, B. O. Roos, B. Schimmelpfennig, M. Schütz, L. Seijo, L. Serrano-Andrés, P. E. M. Siegbahn, J. Stårling, T. Thorsteinsson, V. Veryazov, and P.-O. Widmark, Lund University, Sweden, 2000.
[27] COLUMBUS suite of programs. (ARGOS, CNVRT, SCFPQ, LSTRN, CGDBG, and CIDBG.) R. M. Pitzer (principal author). See A.H.H. Chang and R.M. Pitzer, J. Am. Chem. Soc. **111**, 2500 (1989), and references therein for a description. CNVRT and LSTRN have been adapted to handle ECPAIMP integrals by L. Seijo. CIDBG has been modified for spin-free-state-shifted spin-orbit CI calculations by M. Casarrubios.
[28] R. McWeeny, Proc. R. Soc. London, Ser. A **253**, 242 (1959); Rev. Mod. Phys. **32**, 335 (1960); M. Kleiner and R. McWeeny, Chem. Phys. Lett. **19**, 476 (1973); R. McWeeny, *Methods of Molecular Quantum Mechanics* (Academic, London, 1989).
[29] S. Huzinaga and A.A. Cantu, J. Chem. Phys. **55**, 5543 (1971); S. Huzinaga, D. McWilliams, and A.A. Cantu, Adv. Quantum Chem. **7**, 187 (1973).
[30] Z. Barandiarán and L. Seijo, in *Studies in Physical and Theoretical Chemistry: Vol. 77(B), Computational Chemistry: Structure, Interactions and Reactivity*, edited by S. Fraga (Elsevier, Amsterdam, 1992), p. 435.
[31] B.G. Dick and A.W. Overhauser, Phys. Rev. **112**, 90 (1958).
[32] H.M. Evjen, Phys. Rev. **39**, 675 (1932).
[33] Z. Barandiarán and L. Seijo, Can. J. Chem. **70**, 409 (1992).
[34] J. Andzelm, M. Klobukowsky, E. Radzio-Andzelm, Y. Sakai, and H. Tatewaki, *Gaussian Basis Sets for Molecular Calculations* (Elsevier, Amsterdam, 1984).
[35] P.J. Hay, J. Chem. Phys. **66**, 4377 (1977).
[36] L. G. M. Pettersson (private communication).
[37] T. H. Dunning, Jr. and P. J. Hay, in *Modern Theoretical Chemistry*, edited by H. F. Schaeffer III (Plenum, New York).
[38] J.L. Pascual, L. Seijo, and Z. Barandiarán, J. Chem. Phys. **98**, 9715 (1993).
[39] K. Pierloot and L.G. Vanquickenborne, J. Chem. Phys. **93**, 4154 (1990).
[40] F. Rakowitz, M. Casarrubios, L. Seijo, and C.M. Marian, J. Chem. Phys. **108**, 7980 (1998).
[41] M. Casarrubios and L. Seijo, J. Chem. Phys. **110**, 784 (1999).
[42] S. Díaz-Megías and L. Seijo, Chem. Phys. Lett. **299**, 613 (1999).
[43] L. Seijo and Z. Barandiarán, J. Chem. Phys. **115**, 5554 (2001).
[44] R.D. Shannon, Acta Crystallogr., Sect. B: Struct. Crystallogr. Cryst. Chem. **32**, 751 (1976).
[45] J.L. Pascual, Z. Barandiarán, and L. Seijo, J. Mol. Struct.: THEOCHEM **537**, 151 (2001).
[46] A. Al-Abdalla, Z. Barandiarán, L. Seijo, and R. Lindh, J. Chem. Phys. **108**, 2005 (1998).
[47] C.H. Perry and E.F. Young, J. Appl. Phys. **38**, 4616 (1967).
[48] I. B. Bersuker, *The Jahn-Teller Effect and Vibronic Interactions in Modern Chemistry* (Plenum Press, New York and London, 1984).
[49] M.D. Sturge and H.J. Guggenheim, Phys. Rev. B **4**, 2092 (1971).
[50] M.D. Sturge, Phys. Rev. B **1**, 1005 (1970).
[51] F.S. Ham, Phys. Rev. **138**, A1727 (1965).
[52] E.J. Heller, J. Chem. Phys. **62**, 1544 (1975).
[53] E.J. Heller, Acc. Chem. Res. **14**, 368 (1981).
[54] M.D. Sturge, Phys. Rev. B **8**, 6 (1973).